Plasmon-enhanced light-driven water oxidation by a dye-sensitized photoanode

Degao Wang[a], Benjamin D. Sherman[a,1], Byron H. Farnum[a,2], Matthew V. Sheridan[a], Seth L. Marquard[a], Michael S. Eberhart[a], Christopher J. Dares[b,3], and Thomas J. Meyer[a,3]

[a]Department of Chemistry, University of North Carolina at Chapel Hill, Chapel Hill, NC 27599; and [b]Department of Chemistry and Biochemistry, Florida International University, Miami, FL 33199

Contributed by Thomas J. Meyer, August 5, 2017 (sent for review May 21, 2017; reviewed by Richard Eisenberg and Joseph T. Hupp)

Dye-sensitized photoelectrosynthesis cells (DSPECs) provide a flexible approach for solar water splitting based on the integration of molecular light absorption and catalysis on oxide electrodes. Recent advances in this area, including the use of core/shell oxide interfacial structures and surface stabilization by atomic layer deposition, have led to improved charge-separation lifetimes and the ability to obtain substantially improved photocurrent densities. Here, we investigate the introduction of Ag nanoparticles into the core/shell structure and report that they greatly enhance light-driven water oxidation at a DSPEC photoanode. Under 1-sun illumination, Ag nanoparticle electrodes achieved high photocurrent densities, surpassing 2 mA cm^{-2} with an incident photon-to-current efficiency of 31.8% under 450-nm illumination.

water oxidation | DSPEC | core/shell | plasmonic | atomic layer deposition

A dye-sensitized photoelectrosynthesis cell (DSPEC) integrates light absorption and catalysis to carry out the oxidation of water coupled to the production of H_2 or reduced carbon products. The photoanode of a DSPEC uses a wide-bandgap semiconductor, typically TiO_2 or SnO_2, as a high surface area scaffold for immobilizing molecular chromophores and catalysts. This approach establishes an interface capable of supporting light-driven charge separation and subsequent catalysis at the electrode surface (1–3).

Recent progress has been made in improving solar conversion efficiencies in DSPEC devices, especially by introducing ITO/TiO_2 and SnO_2/TiO_2 core/shell (ITO = tin-doped indium oxide)-based photoanodes (4–6). Even with the core/shell enhancements, additional increases in efficiency and durability are needed to make DSPEC technology viable. Key factors influencing the efficiency of a DSPEC photoanode include the fraction of light absorbed, the interfacial dynamics leading to the accumulation of multiple oxidative equivalents at a catalyst, and the rate of catalysis for water oxidation at the photoanode (7).

The influence of surface-immobilized Ag or Au nanoparticles on the solar conversion efficiencies of dye-sensitized solar cells (DSSCs) by plasmon-enhanced light absorption has been documented (8–11). The introduction of metallic nanoparticles in a DSSC or related photovoltaic device can influence the photoconversion efficiency in several ways, including near-field coupling of the surface plasmon with the light-absorbing material (9, 10, 12), increasing the optical pathlength through the dye layer by light scattering (13, 14), or by electronic effects arising from the presence of the metal nanoparticles (8). In this work, we incorporate ∼100-nm cubic Ag nanoparticles (Ag NPs) on the surface of FTO|SnO_2/TiO_2 films (FTO = fluorine-doped tin oxide) containing a molecular dye/catalyst surface monolayer and observe a substantial improvement in the photocurrent response of the photoanode. Based on the available evidence, we propose that the improved photocurrent density arises from light capture and concentration by the Ag NPs and their role in enhancing the rate of excitation by dyes lying in close proximity.

The application of surface plasmon near-field enhancement is used here to improve the performance of a dye-sensitized photoanode for carrying out light-driven water oxidation at a photoanode, Eq. **1**.

$$2H_2O \rightarrow O_2 + 4H^+ + 4e^- \quad [1]$$

The approach that we have taken involves incorporation of cubic silver NPs onto a FTO|SnO_2/TiO_2 core–shell mesoporous surface. Silver has proven to be an optimal metal for supporting strong surface plasmons in visible wavelengths due to its low dielectric function, and therefore high quality factor (>10), over this range of the spectrum (15). To protect the Ag NPs from degradation by exposure to solution (16), the Ag NPs were deposited on the SnO_2 surface before forming the TiO_2 shell by atomic layer deposition.

Our experiments show that incorporating Ag NPs significantly enhances the performance of the DSPEC photoanode in comparison with a similarly prepared photoanode without the Ag NPs. The improved performance entailed higher photocurrent densities, above 2 mA cm^{-2} under 1-sun irradiation, without any loss in the faradaic efficiencies for O_2 generation (∼95%). An improved incident photon-to-current efficiency (IPCE) of 31.8% at 450 nm compared with 16.3% of photoanode without Ag NPs was observed for the Ag NP surface.

Results and Discussion

Photoanode Preparation and Characterization. Mesoporous FTO|SnO_2/TiO_2 core–shell electrodes used in this study were prepared as

Significance

Dye-sensitized photoelectrosynthesis cells (DSPECs) provide a basis for artificial photosynthesis and solar fuels production. By combining molecular chromophores and catalysts with high surface area, transparent semiconductor electrodes, a DSPEC provides the basis for light-driven conversion of water to O_2 and H_2 or for reduction of CO_2 to carbon-based fuels. The incorporation of plasmonic cubic silver nanoparticles, with a strongly localized surface plasmon absorbance near 450 nm, to a DSPEC photoanode induces a great increase in the efficiency of water oxidation to O_2 at a DSPEC photoanode. The improvement in performance by the molecular components in the photoanode highlights a remarkable advantage for the plasmonic effect in driving the $4e^-/4H^+$ oxidation of water to O_2 in the photoanode.

Author contributions: D.W. and T.J.M. designed research; D.W., B.D.S., B.H.F., M.V.S., and S.L.M. performed research; D.W., M.S.E., C.J.D., and T.J.M. analyzed data; and D.W., B.D.S., C.J.D., and T.J.M. wrote the paper.

Reviewers: R.E., University of Rochester; and J.T.H., Northwestern University.

The authors declare no conflict of interest.

[1]Present address: Department of Chemistry and Biochemistry, Texas Christian University, Fort Worth, TX 76129.

[2]Present address: Department of Chemistry and Biochemistry, Auburn University, Auburn, AL 36849.

[3]To whom correspondence may be addressed. Email: cdares@fiu.edu or tjmeyer@unc.edu.

This article contains supporting information online at www.pnas.org/lookup/suppl/doi:10.1073/pnas.1708336114/-/DCSupplemental.

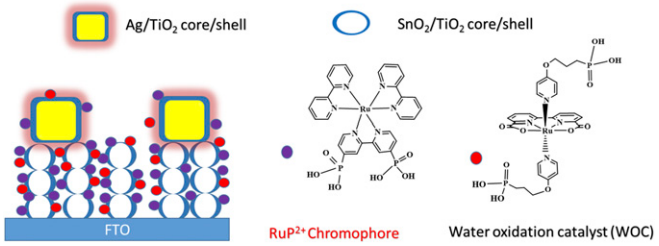

Fig. 1. Illustration of the electrode surface following deposition of cubic Ag NPs on a SnO_2/TiO_2 core/shell surface and loading of the RuP^{2+} chromophore and WOC catalyst to give the FTO|SnO_2/AgNP/TiO_2|–RuP^{2+}/WOC assembly. (*Right*) The structures of the RuP^{2+} chromophore and WOC catalyst are shown.

described elsewhere (4). Fig. S1 shows the image of 3.0-nm TiO_2 shell coating Ag particles. Different mesoporous layer thicknesses of 2.2, 4.1, and 8.1 μm were investigated. The effect of oxide layer thickness on the performance of the interface is shown in Fig. S2. As the 4.1-μm electrode gave the highest photocurrent response, the majority of experiments in this study were carried out with ∼4-μm mesoporous electrodes.

The deposition of polyvinylpyrrolidone (PVP)-coated Ag NPs on the SnO_2 film was accomplished by an electrostatic interaction mechanism (9, 17). Briefly, this involved a short dip treatment of the FTO|SnO_2 electrode in piranha solution (3:1 H_2SO_4:H_2O_2), rinsing with deionized water, and then an overnight soak of the electrode in an ethanol solution with 0.05 wt % Ag NPs. After soaking in the Ag NP solution, the electrodes were air dried and underwent atomic layer deposition (ALD) to deposit the TiO_2 shell. This gave the complete FTO|SnO_2/AgNP/TiO_2| core/shell surface. The as-prepared electrodes were immersed in methanol solution containing 2 mM [Ru(4,4′-PO_3H_2-bpy)(4,4′-bpy)$_2$]$^{2+}$ (RuP^{2+}; bpy = 2,2′-bipyridine). After surface adsorption of the RuP^{2+} chromophore, the water oxidation catalyst [Ru(bda)(4-O(CH_2)$_3$P(O_3H_2))-pyr)$_2$] (WOC; pyr = pyridine; bda = 2,2′-bipyridine-6,6′-dicarboxylate) was incorporated onto the surface during a second soaking step in methanol solution containing 1 mM of the complex. Previous work demonstrated that the loading of the RuP^{2+} chromophore on the surface does not preclude the adsorption of the catalyst containing the –(CH_2)$_3$-PO_3H_2 axial anchoring group (18). Fig. 1 illustrates the fully assembled electrode interface, FTO|SnO_2/AgNP/TiO_2|–RuP^{2+}/WOC. As shown previously by UV-visible measurements, these conditions result in a surface layer consisting of 2:1 chromophore:catalyst ratio (18).

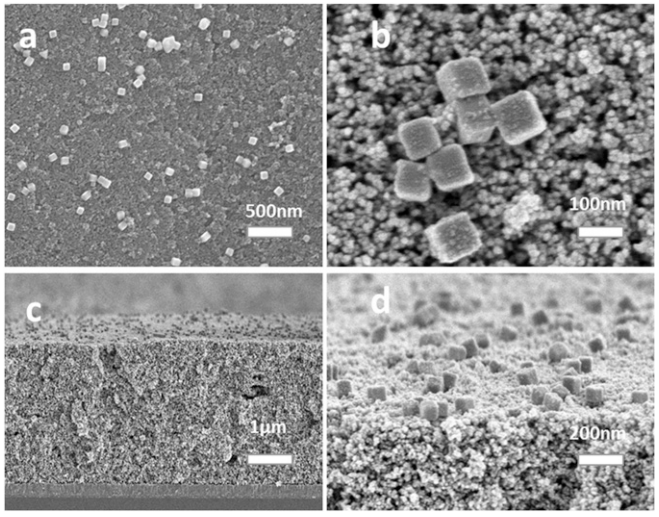

Fig. 2. SEM images of the fully formed photoanode surface. (*A*) Top view of the FTO|SnO_2/AgNP/TiO_2|–RuP^{2+}/WOC film. The Ag NPs are randomly arranged on the oxide surface and do not permeate into the interior of the film. (*B*) Magnified view of *A*. (*C*) Cross-sectional view of the same electrode. (*D*) A 45° angle edge-on-view of the surface.

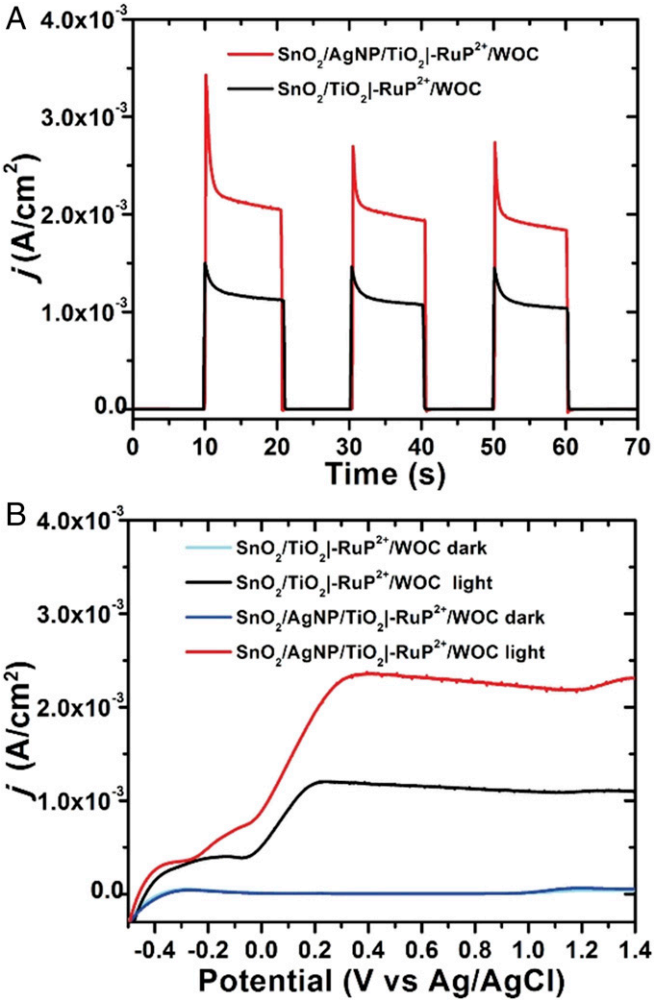

Fig. 3. (*A*) Current–time traces over 10-s dark–light cycles for FTO|SnO_2/TiO_2|–RuP^{2+}/WOC and FTO|SnO_2/AgNP/TiO_2|–RuP^{2+}/WOC electrodes at an applied bias of 0.2 V vs. Ag/AgCl. (*B*) Current density vs. applied voltage curves for the same electrodes under light and dark conditions. White-light illumination at an intensity of 100 mW cm^{-2} was used with a 400-nm cutoff filter. All scans were performed at a scan rate of 50 mV/s. The experiments were carried out in 0.1 M acetic acid/acetate buffer at pH 4.65, 0.4 M in $NaClO_4$.

Fig. 2 shows SEM images of the fully prepared FTO|SnO_2/AgNP/TiO_2|–RuP^{2+}/WOC surface. The 100-nm cubic Ag NPs deposit on the outer surface of the oxide layer, and, as they are larger than the pore openings in the film, it is unlikely that they penetrate within the interior of the film. The 100-nm cubic Ag NPs are randomly dispersed across the top of the oxide layer with both isolated particles and clusters of particles observed. Based on the SEM images, the procedure for depositing the Ag NPs does result in a relatively even distribution across the entire surface.

As mentioned above, treatment of the surface by ALD simultaneously forms a TiO_2 coating on the Ag NPs and forms the SnO_2/TiO_2 core/shell surface in the underlying oxide film. The TiO_2 coating prevents direct contact of the Ag surface with solution (9, 19). The thickness of the TiO_2 surface layer was controlled by varying the number of deposition cycles with each cycle estimated to add 0.06 nm in thickness (20). As summarized in Fig. S3, different

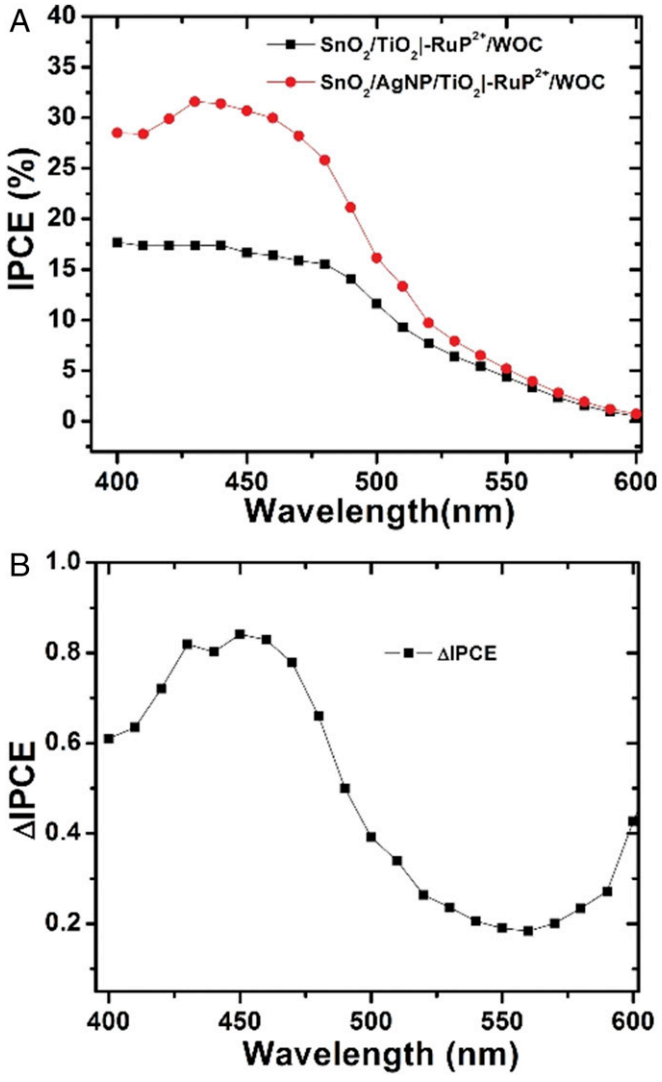

Fig. 4. (*A*) IPCE plots for FTO|SnO_2/TiO_2|–RuP^{2+}/WOC and FTO|SnO_2/AgNP/TiO_2|–RuP^{2+}/WOC. (*B*) The difference in IPCE (ΔIPCE = IPCE with Ag NP minus IPCE without Ag NP) between the two electrodes.

thicknesses of the TiO_2 layer (3.0, 4.5, and 6.0 nm) were explored with the best photocurrent response observed with the 3.0-nm coating. Unless otherwise noted, all samples were prepared with a 3.0-nm TiO_2 shell coating by ALD.

Photochemical Studies. Photocurrent vs. time measurements for FTO|SnO_2/AgNP/TiO_2|–RuP^{2+}/WOC and FTO|SnO_2/TiO_2|–RuP^{2+}/WOC electrodes in pH 4.65 acetate buffer (0.1 M HAc/Ac^-) with 0.4 M $NaClO_4$ as supporting electrolyte were performed under a 0.2 V vs. Ag/AgCl bias with a Pt mesh counter electrode (Fig. 3). All measurements were performed with 100-mW cm^{-2} white light (1 sun) irradiation with a 400-nm cutoff filter to avoid direct bandgap excitation of the oxide. The effect of Ag NPs on the photocurrent is apparent in Fig. 3*A* with nearly a doubling in the current during illumination with the Ag NPs as compared without. In Fig. 3*B*, the overall form of the current–voltage response with or without the Ag NPs is similar but with higher currents from the electrode with added NPs. Importantly, the point of zero current occurs at a similar voltage in both samples, indicating that charging effects of the metal NPs do not contribute to the improved current response (8).

The localized surface plasmon of the Ag NP extends only tens of nanometers from the particle surface and therefore only assemblies

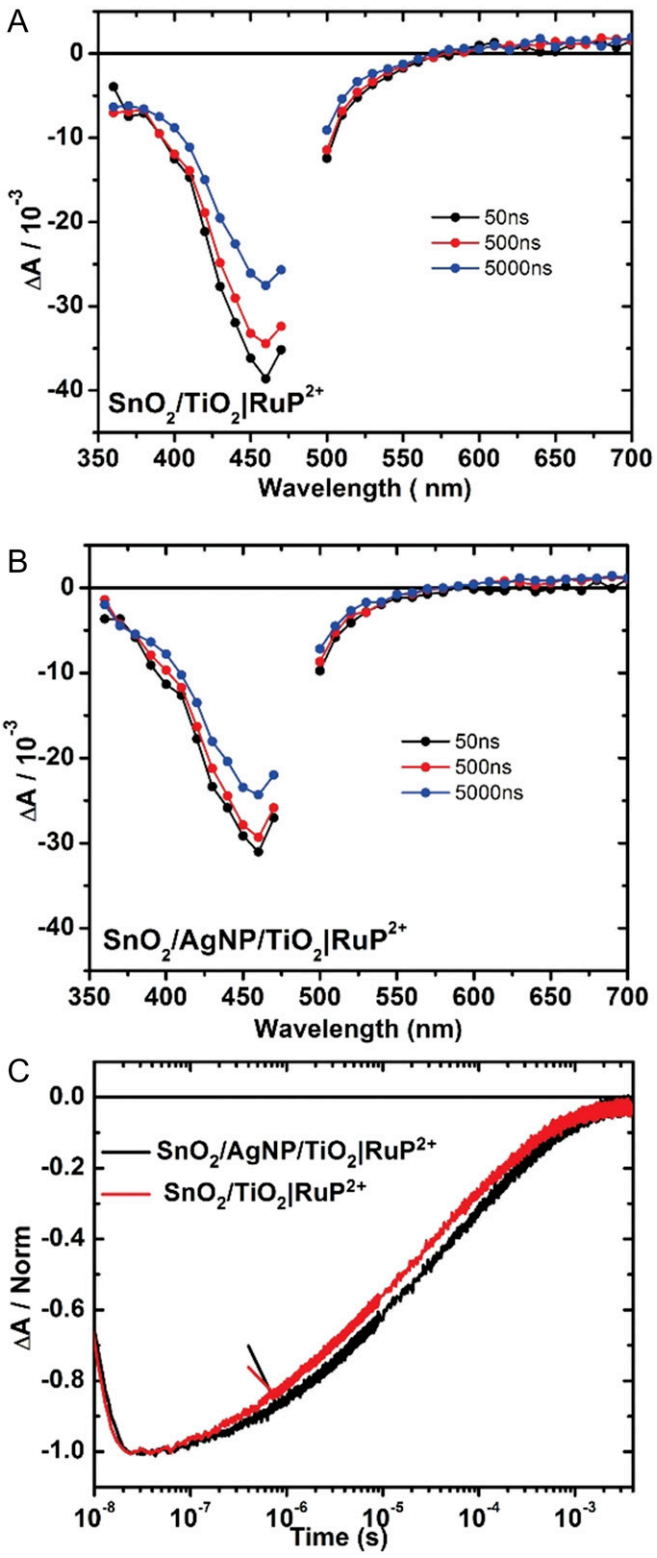

Fig. 5. Nanosecond TA difference spectra recorded following excitation at 532 nm for (*A*) FTO|SnO_2/TiO_2|–RuP^{2+} and (*B*) FTO|SnO_2/AgNP/TiO_2|–RuP^{2+} electrodes. The data in *A* and *B* were recorded in 0.1 M HAc/Ac^- buffer with 0.4 M $NaClO_4$ under an applied bias of 0.2 V vs. Ag/AgCl at room temperature. (*C*) Single-wavelength TA traces at 460 nm for FTO|SnO_2/AgNP/TiO_2|–RuP^{2+} (black) and FTO|SnO_2/TiO_2|–RuP^{2+} (red) recorded in 0.1 M HAc/Ac^- with 0.4 M $NaClO_4$.

at the top of the film, near the Ag NP layer, likely contribute to the improved photocurrent generation (15, 21). Consistent with the localized effect of the plasmon, lower photocurrents were obtained with increasing thickness of the TiO_2 layer applied by ALD. Fig. S3 shows the current response with varying TiO_2 shell thicknesses of 3, 4.5, and 6 nm. The best performance was achieved with a 3-nm TiO_2 coating. Samples prepared with varying thicknesses of the TiO_2 shell, but without the inclusion of Ag NPs, showed little difference in the maximum photocurrent density (Fig. S4).

To assess possible photocurrent generation from the Ag NPs alone, Fig. S5 shows photocurrent measurements for FTO|SnO_2/AgNP/TiO_2|–WOC with no surface-bound chromophore. Without the chromophore, a modest photocurrent of 60 μA cm^{-2} is produced. This indicates that the enhanced photocurrent observed with FTO|SnO_2/AgNP/TiO_2|–RuP^{2+}/WOC is not a result of direct light absorption and sensitization by the Ag NPs. Similar to improvements observed in the performance of DSSCs by the incorporation of Au and Ag NPs, the localized surface plasmon of the Ag NPs improves the rate of excitation of RuP^{2+} chromophores near the NP and leads to higher sustained photocurrents compared with the DSPEC without the Ag NPs (8, 10, 11).

Optical characterization of FTO|SnO_2/AgNP/TiO_2|–RuP^{2+}/WOC and FTO|SnO_2/TiO_2|–RuP^{2+}/WOC electrodes including transmittance, reflectance, and absorptance measurements is shown in Fig. S6. It is notable that the plasmon absorbance of the Ag NP overlaps with the λ_{max} = 450 nm metal-to-ligand charge-transfer (MLCT) absorption band for RuP^{2+} as shown in Fig. S7. This spectral overlap between the chromophore and plasmon resonance of the Ag NP is essential to realizing the improved solar energy conversion of the interface. The IPCE measurements in Fig. 4 highlight the improved light harvesting with the incorporation of the Ag NPs. The IPCE of FTO|SnO_2/AgNP/TiO_2|–RuP^{2+}/WOC reaches 31.8% at 450 nm, a nearly 100% increase over the IPCE for FTO|SnO_2/TiO_2|–RuP^{2+}/WOC (16.3%) at this same wavelength. The difference spectrum comparing the IPCE with the Ag NPs minus the IPCE without the Ag NPs is shown in Fig. 4*B*. From these data, improved light harvesting of the surface with the Ag NPs occurs over wavelengths corresponding to the MLCT excitation of RuP^{2+}. This reiterates that the increased photocurrents are a result of improved light capture by the chromophore through interaction with the surface plasmon of the Ag NP as opposed to a direct effect of the Ag NP. The IPCE value for FTO|SnO_2/AgNP/TiO_2|–RuP^{2+}/WOC represents one of the highest yet observed for a RuP^{2+}-based DSPEC at 450 nm (4, 22, 23).

Light-Driven Water Oxidation. A collector-generator method (24) was used to investigate light-driven O_2 production as shown in Fig. S8. These studies revealed essentially the same faradaic efficiency for O_2 production by FTO|SnO_2/TiO_2|–RuP^{2+}/WOC and FTO|SnO_2/AgNP/TiO_2|–RuP^{2+}/WOC electrodes (96% and 94%, respectively). During 15-min illumination periods, the photocurrent of both FTO|SnO_2/TiO_2|–RuP^{2+}/WOC and FTO|SnO_2/AgNP/TiO_2|–RuP^{2+}/WOC decreased to half of their initial values. This result is consistent with previous observations using similar chromophore/catalyst interfaces, and the presence of the Ag NP does not appear to influence the surface stability of the film (4). The high faradaic efficiency for O_2 generation with or without the Ag NPs indicates the presence of the metal NPs does not affect the functionality of the catalyst. The substantially higher photocurrents with added Ag NPs are consistent with a plasmon enhancement of chromophores near the NPs, which likely enables higher turnover frequencies of nearby catalysts enabling the higher current densities.

Transient Absorption Studies. The results of transient absorption (TA) measurements were used to investigate interfacial electron transfer dynamics. The TA measurements were performed under an applied bias of 0.2 V vs. Ag/AgCl at pH 4.65 in 0.1 M acetate buffer 0.4 M in $NaClO_4$. Difference spectra for FTO|SnO_2/TiO_2|–RuP^{2+} and FTO|SnO_2/AgNP/TiO_2|–RuP^{2+} from 350 to 700 nm following excitation at 532 nm are shown in Fig. 5 *A* and *B*. In both Fig. 5 *A* and *B*, the spectra are consistent with excitation followed by rapid, <10-ns injection to give the oxidized chromophore, –RuP^{3+}. With or without the presence of the Ag NPs, rapid loss of the characteristic MLCT absorption at λ_{max} = 450 nm evidences the loss of ground state and formation of the oxidized dye.

The bleaching recovery traces shown in Fig. 5*C* reveal similar lifetimes for photooxidized RuP^{3+} in the presence or absence of the Ag NPs, 25 and 16 μs, respectively, as measured by the time required for half of the absorption feature to decay to zero. Based on the similar lifetime data, the presence of the Ag NPs does not appear to affect either the sensitization of the oxide by RuP^{2+*} or the recombination of injected electrons to the oxidized RuP^{3+}. While not offering direct evidence, taken in concert with the decrease in transmittance (Fig. S6*A*) and increase in absorptance (Fig. S6*D*), these observations do support the conclusion that the Ag NPs contribute to the improved performance by plasmon-enhanced light absorption of the RuP^{2+} sensitizer.

Conclusion. Our results are consistent with localized surface plasmon-enhanced light harvesting by including Ag NPs in the DSPEC photoanode surface. From the photocurrent and TA measurements, photoinduced electron injection and back-electron transfer are unaffected by the presence of the Ag NPs. However, the introduction of the Ag NPs leads to a nearly twofold increase in the photocurrent generated by the interface under identical conditions. Our results are important in understanding and extending the plasmonic enhancement of molecular light absorption to DSPEC water oxidation applications. The Ag NPs show no detrimental effect on the DSPEC device stability or faradaic efficiency for light-driven water oxidation. The addition of Ag NPs enhances light absorption of the MLCT RuP^{2+} dye and leads to an increase in the IPCE with a maximum of 31.8% at 450 nm. The plasmonic DSPEC produces a photocurrent density above 2 mA cm^{-2} after 30 s of illumination with 1 sun simulated solar light. At the microscopic level, the impact of the plasmonic effect is extraordinary. Additional improvements in light collection maybe possible by varying the surface architectures to integrate a greater population of immobilized RuP^{2+} sensitizers in close proximity to the Ag NPs.

ACKNOWLEDGMENTS. This work was funded through a Department of Energy (DOE) Nuclear Energy University Program award, under Contract DE-NE0008539. A portion of this work was performed using IPCE and Nanosecond Transient Absorption instrumentation in the University of North Carolina (UNC) Energy Frontier Research Center (EFRC) Instrumentation Facility established by the UNC EFRC: Center for Solar Fuels, an EFRC funded by the US DOE, Office of Science, Office of Basic Energy Sciences under Award DE-SC0001011. This work was performed in part at the Chapel Hill Analytical and Nanofabrication Laboratory, a member of the North Carolina Research Triangle Nanotechnology Network, which is supported by the NSF, Grant ECCS-1542015, as part of the National Nanotechnology Coordinated Infrastructure.

1. Youngblood WJ, Lee SHA, Maeda K, Mallouk TE (2009) Visible light water splitting using dye-sensitized oxide semiconductors. *Acc Chem Res* 42: 1966–1973.
2. House RL, et al. (2015) Artificial Photosynthesis: Where are we now? Where can we Go? *J Photochem Photobiol Photochem Rev* 25:32–45.
3. O'Regan B, Gratzel MA (1991) Low-cost, high-efficiency solar cell based on dye-sensitized colloidal TiO_2 films. *Nature* 353:737–740.
4. Sherman BD, et al. (2015) Light-driven water splitting with a molecular electroassembly-based core/shell photoanode. *J Phys Chem Lett* 6:3213–3217.
5. Alibabaei L, Sherman BD, Norris MR, Brennaman MK, Meyer TJ (2015) Visible photoelectrochemical water splitting into H_2 and O_2 in a dye-sensitized photoelectrosynthesis cell. *Proc Natl Acad Sci USA* 112:5899–5902.
6. Wang D, et al. (2017) Inner layer control of performance in a dye-sensitized photoelectrosynthesis cell. *ACS Appl Mater Interfaces*, 10.1021/acsami.7b00225.
7. Ashford DL, et al. (2015) Molecular chromophore-catalyst assemblies for solar fuel applications. *Chem Rev* 115:13006–13049.
8. Choi H, Chen WT, Kamat PV (2012) Know thy nano neighbor. Plasmonic versus electron charging effects of metal nanoparticles in dye-sensitized solar cells. *ACS Nano* 6:4418–4427.

9. Standridge SD, Schatz GC, Hupp JT (2009) Distance dependence of plasmon-enhanced photocurrent in dye-sensitized solar cells. *J Am Chem Soc* 131:8407–8409.
10. Brown MD, et al. (2011) Plasmonic dye-sensitized solar cells using core-shell metal-insulator nanoparticles. *Nano Lett* 11:438–445.
11. Zarick HF, et al. (2016) Improving light harvesting in dye-sensitized solar cells using hybrid bimetallic nanostructures. *ACS Photonics* 3:385–394.
12. Atwater HA, Polman A (2010) Plasmonics for improved photovoltaic devices. *Nat Mater* 9:205–213.
13. Fang C, et al. (2014) (Gold core)/(titania shell) nanostructures for plasmon-enhanced photon harvesting and generation of reactive oxygen species. *Energy Environ Sci* 7:3431–3438.
14. Kakavelakis G, et al. (2016) Plasmonic backscattering effect in high-efficient organic photovoltaic devices. *Adv Energy Mater* 6:1501640.
15. Rycenga M, et al. (2011) Controlling the synthesis and assembly of silver nanostructures for plasmonic applications. *Chem Rev* 111:3669–3712.
16. Saliba M, et al. (2015) Plasmonic-induced photon recycling in metal halide perovskite solar cells. *Adv Funct Mater* 25:5038–5046.
17. Wang Z, Chumanov G (2003) WO_3 sol–gel modified Ag nanoparticle arrays for electrochemical modulation of surface plasmon resonance. *Adv Mater* 15:1285–1289.
18. Sheridan MV, et al. (2016) Evaluation of chromophore and assembly design in light-driven water splitting with a molecular water oxidation catalyst. *ACS Energy Lett.* 1:231–236.
19. Qi J, Dang X, Hammond PT, Belcher AM (2011) Highly efficient plasmon-enhanced dye-sensitized solar cells through metal@oxide core-shell nanostructure. *ACS Nano* 5: 7108–7116.
20. Lapides AM, et al. (2015) Synthesis, characterization, and water oxidation by a molecular chromophore-catalyst assembly prepared by atomic layer deposition. The "Mummy" strategy. *Chem Sci (Camb)* 6:6398–6406.
21. Barnes WL, Dereux A, Ebbesen TW (2003) Surface plasmon subwavelength optics. *Nature* 424:824–830.
22. Coppo RL, Farnum BH, Sherman BD, Murakami Iha NY, Meyer TJ (2017) The role of layer-by-layer, compact TiO2 films in dye-sensitized photoelectrosynthesis cells. *Sustainable Energy Fuels* 1:112–118.
23. Gao Y, et al. (2013) Visible light driven water splitting in a molecular device with unprecedentedly high photocurrent density. *J Am Chem Soc* 135:4219–4222.
24. Sherman BD, Sheridan MV, Dares CJ, Meyer TJ (2016) Two electrode collector-generator method for the detection of electrochemically or photoelectrochemically produced O_2. *Anal Chem* 88:7076–7082.
25. Ashford DL, Sherman BD, Binstead RA, Templeton JL, Meyer TJ (2015) Electro-assembly of a chromophore–catalyst bilayer for water oxidation and photocatalytic water splitting. *Angew Chem* 127:4860.